Analysis of the x-ray spectra emitted by laser-produced plasma of highly ionized lanthanum and praseodymium in the 8.4 to 12.0 Å wavelength range

1994 Phys. Scr. 50 61

(http://iopscience.iop.org/1402-4896/50/1/008)

Physica Scripta. Vol. 50, 61–67, 1994

Analysis of the X-Ray Spectra Emitted by Laser-Produced Plasma of Highly Ionized Lanthanum and Praseodymium in the 8.4 to 12.0 Å Wavelength Range

A. Zigler, P. Mandelbaum, J. L. Schwob and D. Mitnik

Racah Institute of Physics, The Hebrew University, 91904 Jerusalem, Israel

Received October 28, 1993; accepted in revised form January 10, 1994

Abstract

A detailed analysis of the X-ray spectra emitted by laser produced plasma of lanthanum (8.5–12.5 Å) and praseodymium (8.4–11.3 Å) is given, using *ab-initio* calculations with the HULLAC relativistic code. Resonance $3d$–nf ($n = 4, 5, 6$) and $3p$–$4s$, $4d$ transitions of the La XXX and Pr XXXII Ni I-like ions and neighbouring ionization states (La XXVIII to La XXXVI, Pr XXX to Pr XXXVI) have been identified.

1. Introduction

Laser-produced plasmas of high-Z elements are powerful sources of radiation in the X-ray region. Theoretical analysis of the radiation emitted from these dense plasmas is useful for understanding the plasma energetics and the determination of plasma parameters from spectroscopic diagnostic. Recently, many such spectra emitted by ions in ionization states isoelectronic to Ni I and neighbouring isoelectronic sequences have been obtained and analysed for heavy elements up to uranium [1–10]. Such spectra emitted by the rare earths plasmas can be used as a bright source in the 1 keV energy range. However, only limited work has been done on these spectra since the pioneering work of Bulkhalter *et al.* [11], besides the analysis of highly ionized europium from laser-produced plasma [12] and of gadolinium introduced in the PLT Tokamak [13]. Also a brief account of similar spectra of Sm, Gd, Tb and Ho with an emphasis on the Ni I-like transitions has been published recently [14]. The interest in these spectra for the study of inner shell excited autoionizing configurations [15], prompted us to make a detailed analysis of the lanthanum and praseodymium spectra obtained at the Soreq Nuclear Center [16]. Also the $3d$–$4f$ pseudocontinuum emitted by the highly ionized praseodymium ions in this region has been used recently as a continuum source in time-resolved absorption experiments [17].

2. Experiment

Spectra of lanthanum and praseodymium were obtained using laser produced plasmas at the Soreq Nuclear Research Center. The laser pulse energy was varied between 3 and 70 J, while the laser pulse duration of 3.5 ns was kept constant. The beam was focused by a lens onto a plane target. The X-rays were dispersed by a KAP crystal and recorded on RAR 2495 films. The wavelengths were calibrated using known K-shell lines and their satellites of He I- and Li I-like sodium, providing the wavelength measurements at an accuracy of about 3 mÅ. Figure 1 displays a typical microdensitometer recording of a lanthanum spectrum emitted by a plasma obtained with a 3 J laser pulse. Figure 2 shows a praseodymium spectrum obtained from a 5 J laser pulse.

3. Theory

The spectra were analyzed by comparison of *ab-initio* computed wavelengths and gf values to experimental wavelengths and intensities. The relativistic-parametric-potential [18] method for *ab-initio* wavelengths and transition probabilities calculations was used. Because of the accuracy of the theoretical predictions and the isoelectronic regularities there is no ambiguity in most cases in the identification of lines, besides the blendings. For the identification of $3d^n$–$3d^{n-1}nf$ transitions, which appear in the spectra as single unresolved features, use has been made of the UTA (Unresolved Transition Array) model [19]. Unresolved arrays that are split into jj subarrays (i.e. $3d^{10}nl$–$3d^9_j nl4f_{j'}$) were identified using the SOSA (Spin Orbit Split Array) model [20].

4. Results and discussion

The results of the computations and the identification of the lines are given in Table I for lanthanum and in Table II for praseodymium. In these tables, the first column gives a label which identifies the transition (or the transition array) on Fig. 1 (lanthanum spectrum) and on Fig. 2 (praseodymium spectrum). The next two columns show the experimental

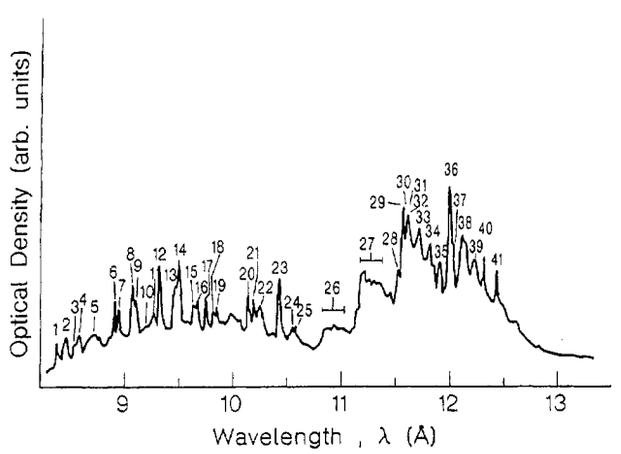

Fig. 1. Microdensitometer recording of the X-ray spectrum emitted by a lanthanum target irradiated with a laser pulse of 3 J nominal energy and 3.5 ns duration. Labels refer to Table I.

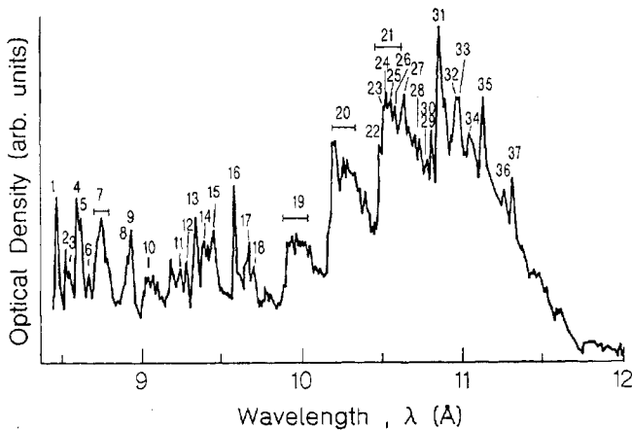

Fig. 2. Microdensitometer recording of the X-ray spectrum emitted by a praseodymium target irradiated with a laser pulse of 5 J nominal energy and 3.5 ns duration. Labels refer to Table II.

wavelength and intensity. In the case of UTA, the mean wavelength of the experimental features is given. The following columns give the isoelectronic sequence of the ion, the theoretical wavelength of the transition [or the weighted mean wavelength, in the case of UTA, followed by the theoretical width of the array (in mÅ)]; the *gf* value of the transition is given in the case of line transition. The last columns give the upper level designation (only the biggest component preceded by the square of the eigenvector is given), the total quantum number J_U of the upper level and J_L of the lower level.

4.1. *Ti I- to Fe I-like ions*

For these ionization states (ground configuration from $3d^4$ to $3d^8$) the experimental spectrum shows a band structure of unresolved transition arrays corresponding to the $3d^n$–$3d^{n-1}4f$ transitions. The experimental wavelength ranges of these bands have been compared to the computed UTA mean wavelengths and widths. The higher ionization states (Ti I-, V I- and Cr I-like) appear, in the lanthanum spectra, only in those spectra obtained with high energy (70 J) laser pulses. These transition do not appear in spectrum displayed in Fig. 1 which was obtained with 3 J laser pulse. This is indicated by (#) in the label column of Table I.

4.2. *Co I-like ions*

The $3p^63d^9$–$3d^63d^8[4f + 5f]$ and $3p^63d^9$–$3p^53d^94d$ transitions were computed *ab-initio* with the RELAC code. The results of these full intermediate coupling calculations are compared in Tables I and II to the partially resolved experimental features.

4.3. *Ni I-like ions*

For the Ni I-like ions the configuration mixing scheme of Tragin *et al.* [10] was used for the theoretical computations using the RELAC code. The $3p^63d^{10}$–$3p^63d^9[4p + 4f] + 3p^53d^{10}[4s + 4d] + 3s^13p^63d^{10}4p$ and $3p^63d^{10}$–$3p^63d^9[5p + 5f + 6p + 6f + 7f] + 3p^53d^{10}[5s + 5d]$ transitions have been calculated. The results of these computations were compared to the prominent lines appearing in the spectra. The discrepancy between calculated and measured wavelength was less than 20 mÅ. As pointed out in Refs [10] and [14], some accidental crossing of levels of the Ni I-like ions can enhance significantly line intensities. This is the case for the $3s^23p^63d^{10}$–$3s^23p^63d^9_{5/2}4f_{5/2}$ [$J = 1$] and $3s^23p^63d^{10}$–$3s3p^63d^{10}4p_{3/2}$ [$J = 1$] transition in Pr XXXII. The *gf* factor of the first transition is enhanced from 0.012 to 0.20 through mixing of the upper level with $3s^23p^5_{3/2}3d^{10}4s$ [$J = 1$] and the second one from 0.14 to 0.61 through mixing of the upper level with $3s^23p^63d^9_{3/2}4f_{5/2}$ [$J = 1$].

4.4. *Cu I- and Zn I-like isoelectronic sequence*

In the spectra of high-Z elements ($Z > 70$) [6, 10], one observes the typical *jj* splitting of the $3d$–nf SOSA transitions ($n > 3$) in Cu I-like and lower ionization states. In particular, this gives rise to two very well observed "grids" of array transitions, the first located on the long wavelength side of the $3d^{10}$–$3d^9_{3/2}4f_{5/2}$ Ni I-like line, and the second one on the long wavelength side of the $3d^{10}$–$3d^9_{5/2}4f_{7/2}$ transition. In a previous work [4], departure from pure *jj* coupling for the $3d$–$4f$ array was reported. This departure is expected to be even stronger for the same arrays of lower-Z elements. In the case of the La and Pr spectra, only one grid of array is observed: from the two *jj* subarrays observed in the spectra of high-Z elements only the one satellite to the $3d^{10}$–$3d^9_{3/2}4f_{5/2}$ Ni I-like is still observable (corresponding to the $3d^{10}\,{}^1S_0$–$3d^94f\,{}^1P_1$ transition in *LS* coupling). The transition from pure *jj* to *LS* coupling is further demonstrated by calculating the $3d^{10}4d$–$3d^94d4f$ transitions in ions along the Cu I-like isoelectronic sequence. The resulting synthetic spectrum is displayed in Fig. 3 for La [Fig. 3(a)], Dy [Fig. 3(b)] and Pt [Fig. 3(c)]. As Z increases the intensity of the second array increases (this array corresponds to the $3d^{10}$–$3d^9_{5/2}4f_{7/2}$ transition in the Ni I-like ion). Thus, for the $3d$–$4f$ transitions of the Cu I- and Zn I-like isoelectronic only one SOSA was observed and identified in Tables I and II. In the other $3d$–nf transitions with $n > 4$, however, the two different *jj* subarrays were identified. This split is illustrated in Fig. 4 for the $3d^{10}4d$–$3d^94d5f$ transitions in Cu I-like lanthanum. For the $3d$–$4f$ transitions, another complication arising from the non-relativistic configuration mixing, can put into question the simple identification of features 38, 39 (in the lanthanum spectrum) or 33, 34 (in the praseodymium spectrum) as pertaining to $3d$–$4f$ transitions in the Cu I- and Zn I-like ions, respectively. Table III shows the effect of configuration mixing on the computations of the $3d^{10}4s$–$3d^94s4f$ transition. Presented in Table III(a) are the results for the single configuration computation. Table III(b) gives the results when configuration mixing of the upper configuration with $3d^94p4d$ is introduced. Table IV shows the effect of configuration mixing on the $3d^{10}4p$–$3d^94p4f$ transition. Identification of these theoretical computed lines in the experimental spectra would be possible only if much higher spectral resolution could be achieved. Considering that the wavelength difference between the bands is about 100 mÅ, it is clear, however, that the configuration mixing can shift some intense lines from the original band to the adjacent feature. This effect was considered when giving the classification in Tables I and II. Nevertheless it can be shown that the intensity of the band 38 (La spectrum) or 33 (Pr spectrum) is contributed mainly by Cu I-like transitions. This was demonstrated by performing a level population calculation based on a collisional model that included the low lying $3d^{10}4l$ and $3d^{10}5l$ ($l = s, p, d, f$) levels of the Cu I-

Table I. *Results for identified transitions in the spectrum of lanthanum laser-produced plasma (8.5–12.5 Å)*

Label	λ_{exp} (Å)	I_{exp}	Sequence	λ_{th} (Å)	$\Delta\lambda_{th}$ (mÅ)	gf_{th}	Upper level or UTA transition	J_U	J_L
1	8.544	10	Ni I	8.547		0.42	0.89 $[3d^9_{3/2}6f_{5/2}]$	1	0
2	8.614	8	Cu I	8.627	2		$3d^{10}4s$–$3d^9_{3/2}4s6f_{5/2}$(*)		
3	8.730	3	Cu I	8.733	5		$3d^{10}4s$–$3d^9_{5/2}4s6f_{7/2}$(*)		
4	8.800	7	Zn I	8.810		0.59	0.89 $[3d^9_{3/2}4s^26f_{5/2}]$(*)	1	0
5	8.915	5	Zn I	8.920		0.43	0.79 $[3d^9_{5/2}4s^26f_{7/2}]$(*)	1	0
6	9.041	25	Co I	9.047		3.48	0.79 $[3d^3_{3/2}3d^5_{5/2}(4)5f_{5/2}]$	7/2	5/2
				9.047		2.45	0.67 $[3d^3_{3/2}3d^5_{5/2}(4)5f_{5/2}]$	5/2	5/2
				9.046		0.81	0.58 $[3d^3_{3/2}3d^5_{5/2}(4)5f_{5/2}]$	3/2	5/2
				9.056		0.79	0.39 $[3d^3_{3/2}3d^5_{5/2}(4)5f_{7/2}]$	3/2	5/2
7	9.073	15	Co I	9.076		2.66	0.39 $[3d^3_{3/2}3d^5_{5/2}(2)5f_{5/2}]$	5/2	3/2
				9.077		1.92	0.82 $[3d^2_{3/2}3d^6_{5/2}(2)5f_{5/2}]$	3/2	3/2
				9.091		0.67	0.55 $[3d^3_{3/2}3d^5_{5/2}(2)5f_{5/2}]$	7/2	5/2
8	9.200	20	Co I	9.196		1.03	0.74 $[3d^4_{3/2}3d^4_{5/2}(2)5f_{7/2}]$	7/2	5/2
			Ni I	9.200	7		$3d^94s$–$3d^84s5f$		
9	9.227	10	Ni I	9.230	16		$3d^94s$–$3d^84s5f$		
10	9.321	3	Ni I	9.308	64		$3d^94s$–$3d^84s5f$		
11	9.380	6	Ni I	9.379	64		$3d^94s$–$3d^84s5f$		
				9.359		0.14	0.99 $[3s3p^63d^{10}4p_{3/2}]$	1	0
12	9.433	30	Ni I	9.448		1.21	0.89 $[3d^9_{3/2}5f_{5/2}]$	1	0
13	9.567	15	Ni I	9.585		0.48	0.79 $[3d^9_{5/2}5f_{7/2}]$	1	0
14	9.603	25	Cu I	9.627	5		$3d^{10}4s$–$3d^9_{3/2}4s5f_{5/2}$(*)		
15	9.740	7	Cu I	9.744	8		$3d^{10}4s$–$3d^9_{5/2}4s5f_{7/2}$(*)		
16	9.774	10	Zn I	9.774		1.47	0.89 $[3d^9_{3/2}4s^25f_{5/2}]$(*)	1	0
17	9.841	10	Ni I	9.833		0.45	0.97 $[3p^5_{1/2}3d^{10}4d_{3/2}]$	1	0
18	9.912	5	Zn I	9.920		0.49	0.79 $[3d^9_{5/2}4s^25f_{7/2}]$(*)	1	0
19	9.945	8	Cu I	9.920		0.41	0.50 $[3p^5_{1/2}3d^{10}4s(1)4d_{3/2}]$	3/2	1/2
				9.928		0.29	0.99 $[3p^5_{1/2}3d^{10}4s(1)4d_{3/2}]$	1/2	1/2
20	10.217	15	Co I	10.192		0.93	0.59 $[3p^5_{3/2}3d^9_{3/2}(1)4d_{5/2}]$	5/2	3/2
				10.207		0.41	0.43 $[3p^5_{3/2}3d^9_{3/2}(1)4d_{3/2}]$	1/2	3/2
				10.207		0.81	0.58 $[3p^5_{3/2}3d^9_{3/2}(3)4d_{5/2}]$	3/2	3/2
				10.214		0.47	0.62 $[3p^5_{3/2}3d^9_{5/2}(3)4d_{5/2}]$	5/2	5/2
21	10.266	12	Co I	10.248		0.69	0.41 $[3p^5_{3/2}3d^9_{5/2}(3)4d_{3/2}]$	3/2	5/2
				10.251		0.41	0.31 $[3p^5_{3/2}3d^9_{3/2}(3)4d_{3/2}]$	5/2	3/2
				10.264		0.54	0.54 $[3p^5_{3/2}3d^9_{3/2}(2)4d_{5/2}]$	5/2	3/2
22	10.340	8	Co I	10.333		0.40	0.45 $[3p^5_{3/2}3d^9_{5/2}(2)4d_{3/2}]$	3/2	5/2
				10.340		0.64	0.47 $[3p^5_{3/2}3d^9_{5/2}(2)4d_{3/2}]$	5/2	5/2
23	10.512	20	Ni I	10.492		0.98	0.88 $[3p^5_{3/2}3d^{10}4d_{5/2}]$	1	0
24	10.621	6	Cu I	10.597		0.98	0.91 $[3p^5_{3/2}3d^{10}4s(1)4d_{5/2}]$	3/2	1/2
25	10.658	6	Cu I	10.633		0.33	0.76 $[3p^5_{3/2}3d^{10}4s(1)4d_{3/2}]$	1/2	1/2
(#)	10.095		Ti I	10.083	248		$3d^4$–$3d^34f$		
(#)	10.360		V I	10.356	259		$3d^5$–$3d^44f$		
(#)	10.660		Cr I	10.646	264		$3d^6$–$3d^54f$		
26	11.010		Mn I	10.955	269		$3d^7$–$3d^64f$		
27	11.315		Fe I	11.286	266		$3d^8$–$3d^74f$		
28	11.570	7	Co I	11.558		7.6	0.67 $[3d^2_{3/2}3d^6_{5/2}(0)4f_{5/2}]$	5/2	3/2
29	11.611	20	Co I	11.595		14.9	0.21 $[3d^3_{3/2}3d^5_{5/2}(2)4f_{5/2}]$	7/2	5/2
				11.608		10.2	0.40 $[3d^3_{3/2}3d^5_{5/2}(4)4f_{5/2}]$	5/2	5/2
30	11.644	18	Co I	11.642		7.0	0.62 $[3d^2_{3/2}3d^6_{5/2}(2)4f_{5/2}]$	3/2	3/2
31	11.652	15	Co I	11.643		5.2	0.64 $[3d^3_{3/2}3d^5_{5/2}(4)5f_{5/2}]$	3/2	5/2
32	11.670	10	Co I	11.669		4.3	0.54 $[3d^2_{3/2}3d^6_{5/2}(2)4f_{5/2}]$	5/2	3/2
				11.731		2.8	0.49 $[3d^2_{3/2}3d^6_{5/2}(2)4f_{5/2}]$	1/2	3/2
33	11.787	15	Ni I	11.749	336		$3d^94s$–$3d^84s4f$		
34	11.837	10	Ni I						
35	11.918	10	Cu I	11.964		2.1	0.49 $[3d^9_{3/2}4d_{3/2}(0)4d_{5/2}]$	5/2	3/2
36	12.020	30	Ni I	11.997		6.2	0.68 $[3d^9_{3/2}4f_{5/2}]$	1	0
37	12.047	10	Cu I	12.053		4.8	0.28 $[3d^9_{3/2}4s(1)4f_{5/2}]$	3/2	1/2
38	12.147	20	Cu I	12.228	17		$3d^{10}4s$–$3d^9_{3/2}4s4f_{5/2}$(*)		
39	12.240	10	Zn I	12.252		5.3	0.71 $[3d^9_{3/2}4s^24f_{5/2}]$(*)	1	0
40	12.335	20	Ni I	12.351		0.5	0.55 $[3d^9_{5/2}4f_{7/2}]$	1	0
41	12.458	20	Ni I	12.431		0.5	0.98 $[3p^5_{3/2}3d^{10}4s]$	1	0

(#) Indicates feature observed in spectra obtained with higher energy laser pulses only. (*) Indicates those cases where the experimental feature may arise from the superposition of lines from transitions with different electron spectators configurations. Only the transition with the lowest of these configurations is given (see text).

Table II. *Results for identified transitions in the spectrum of praseodymium laser-produced plasma (8.4–11.3 Å)*

Label	λ_{exp} (Å)	I_{exp}	Sequence	λ_{th} (Å)	$\Delta\lambda_{th}$ (mÅ)	gf_{th}	Upper level or UTA transition	J_U	J_L
1	8.460	25	Ni I	8.447		1.23	0.90 $[3d^9_{3/2}5f_{5/2}]$	1	0
2	8.521	10	Ni I	8.481		0.61	0.99 $[3s4p_{3/2}]$	1	0
3	8.540	5							
4	8.595	25	Cu I	8.610	4		$3d^{10}4s$–$3d^9_{3/2}4s5f_{5/2}$(*)		
5	8.609	25	Ni I	8.589		0.52	0.80 $[3d^9_{5/2}5f_{7/2}]$	1	0
6	8.666	5	Ni I	8.661		0.09	0.90 $[3s4p_{1/2}]$	1	0
7	8.748	15	Cu I	8.723	7		$3d^{10}4s$–$3d^9_{5/2}4s5f_{7/2}$(*)		
			Zn I	8.736		1.43	0.89 $[3d^9_{3/2}4s^25f_{5/2}]$(*)	1	0
				8.754		0.47	0.97 $[3p^5_{1/2}3d^9_{3/2}(1)4d_{3/2}]$	5/2	3/2
			Co I	8.763		0.24	0.53 $[3p^5_{1/2}3d^9_{3/2}(2)4d_{3/2}]$	1/2	3/2
				8.765		0.37	0.81 $[3p^5_{1/2}3d^9_{3/2}(2)4d_{3/2}]$	3/2	3/2
8	8.885	3	Zn I	8.872		0.64	0.79 $[3d^9_{5/2}4s^25f_{7/2}]$(*)	1	0
9	8.915	15	Ni I	8.885		0.47	0.97 $[3p^5_{1/2}3d^{10}4d_{3/2}]$	1	0
10	9.040	3	Cu I	8.966		0.32	0.75 $[3p^5_{3/2}3d^{10}4s(1)4d_{3/2}]$	1/2	1/2
				8.958		0.45	0.48 $[3p^5_{1/2}3d^{10}4s(1)4d_{3/2}]$	3/2	1/2
11	9.225	2	Ni I	9.194		0.03	0.99 $[3d^9_{3/2}5p_{1/2}]$	1	0
12	9.265	5	Ni I	9.246		0.03	0.99 $[3d^9_{5/2}5p_{3/2}]$	1	0
			Co I	9.259		0.39	0.68 $[3p^5_{3/2}3d^9_{5/2}(1)4d_{3/2}]$	5/2	5/2
13	9.314	15	Co I	9.274		0.42	0.66 $[3p^5_{3/2}3d^9_{3/2}(3)4d_{5/2}]$	5/2	3/2
				9.277		0.88	0.71 $[3p^5_{3/2}3d^9_{3/2}(1)4d_{5/2}]$	5/2	3/2
				9.279		1.06	0.74 $[3p^5_{3/2}3d^9_{5/2}(3)4d_{5/2}]$	7/2	5/2
				9.290		0.51	0.45 $[3p^5_{3/2}3d^9_{3/2}(3)4d_{5/2}]$	1/2	3/2
				9.286		0.90	0.58 $[3p^5_{3/2}3d^9_{3/2}(3)4d_{5/2}]$	3/2	3/2
				9.289		0.47	0.63 $[3p^5_{3/2}3d^9_{5/2}(3)4d_{5/2}]$	5/2	5/2
14	9.363	8	Co I	9.322		0.75	0.39 $[3p^5_{3/2}3d^9_{5/2}(3)4d_{3/2}]$	3/2	5/2
				9.332		0.61	0.31 $[3p^5_{3/2}3d^9_{3/2}(2)4d_{5/2}]$	5/2	3/2
15	9.431	12	Co I	9.397		0.48	0.41 $[3p^5_{3/2}3d^9_{5/2}(4)4d_{5/2}]$	3/2	5/2
				9.403		0.80	0.54 $[3p^5_{3/2}3d^9_{5/2}(4)4d_{5/2}]$	5/2	5/2
16	9.559	20	Ni I	9.524		1.03	0.90 $[3p^5_{3/2}3d^{10}4d_{5/2}]$	1	0
17	9.647	8	Cu I	9.616		1.05	0.91 $[3p^5_{3/2}3d^{10}4s(1)4d_{5/2}]$	3/2	1/2
18	9.682	5	Cu I	9.652		0.33	0.76 $[3p^5_{3/2}3d^{10}4s(1)4d_{3/2}]$	1/2	1/2
			Cr I	9.673	244		$3d^6$–$3d^54f$		
19	9.955		Mn I	9.929	248		$3d^7$–$3d^64f$		
20	10.210		Fe I	10.214	247		$3d^8$–$3d^74f$		
21	10.512		Co I	10.519	237		$3d^9$–$3d^84f$		
22	10.474	30	Co I	10.443		8.0	0.67 $[3d^2_{3/2}3d^6_{5/2}(0)4f_{5/2}]$	5/2	3/2
23	10.503	50	Co I	10.473		13.6	0.22 $[3d^3_{3/2}3d^5_{5/2}(2)4f_{5/2}]$	7/2	5/2
24	10.515	60	Co I	10.485		10.4	0.41 $[3d^3_{3/2}3d^5_{5/2}(4)4f_{5/2}]$	5/2	5/2
25	10.542	50	Co I	10.517		7.0	0.65 $[3d^2_{3/2}3d^6_{5/2}(2)4f_{5/2}]$	3/2	3/2
				10.513		5.3	0.67 $[3d^3_{3/2}3d^5_{5/2}(4)5f_{5/2}]$	3/2	5/2
26	10.562	50	Co I	10.540		4.1	0.56 $[3d^2_{3/2}3d^6_{5/2}(2)4f_{5/2}]$	5/2	3/2
27	10.622	25	Co I	10.598		2.7	0.56 $[3d^2_{3/2}3d^6_{5/2}(2)4f_{5/2}]$	1/2	3/2
28	10.714	10	Ni I	10.607	303		$3d^94s$–$3d^84s4f$		
29	10.768	5							
30	10.801	15	Cu I	10.780		2.3	0.49 $[3d^9_{3/2}4d_{3/2}(0)4d_{5/2}]$	5/2	3/2
31	10.852	80	Ni I	10.804		6.3	0.70 $[3d^9_{3/2}4f_{5/2}]$	1	0
			Cu I	10.841		4.4	0.25 $[3d^9_{3/2}4s(1)4f_{5/2}]$	3/2	1/2
32	10.908	40	Cu I	10.998	14		$3d^{10}4s$–$3d^9_{3/2}4s4f_{5/2}$(*)		
33	10.965	40							
34	11.048	20	Zn I	11.021		5.4	0.73 $[3d^9_{3/2}4s^24f_{5/2}]$(*)	1	0
35	11.129	30	Ni I	11.108		0.7	0.58 $[3d^9_{5/2}4f_{7/2}]$	1	0
36	11.256	10	Ni I	11.238		0.2	0.58 $[3d^9_{5/2}4f_{5/2}]$	1	0
37	11.310	10	Ni I	11.314		0.2	0.69 $[3p^5_{3/2}3d^{10}4s]$	1	0

(*) As in Table I.

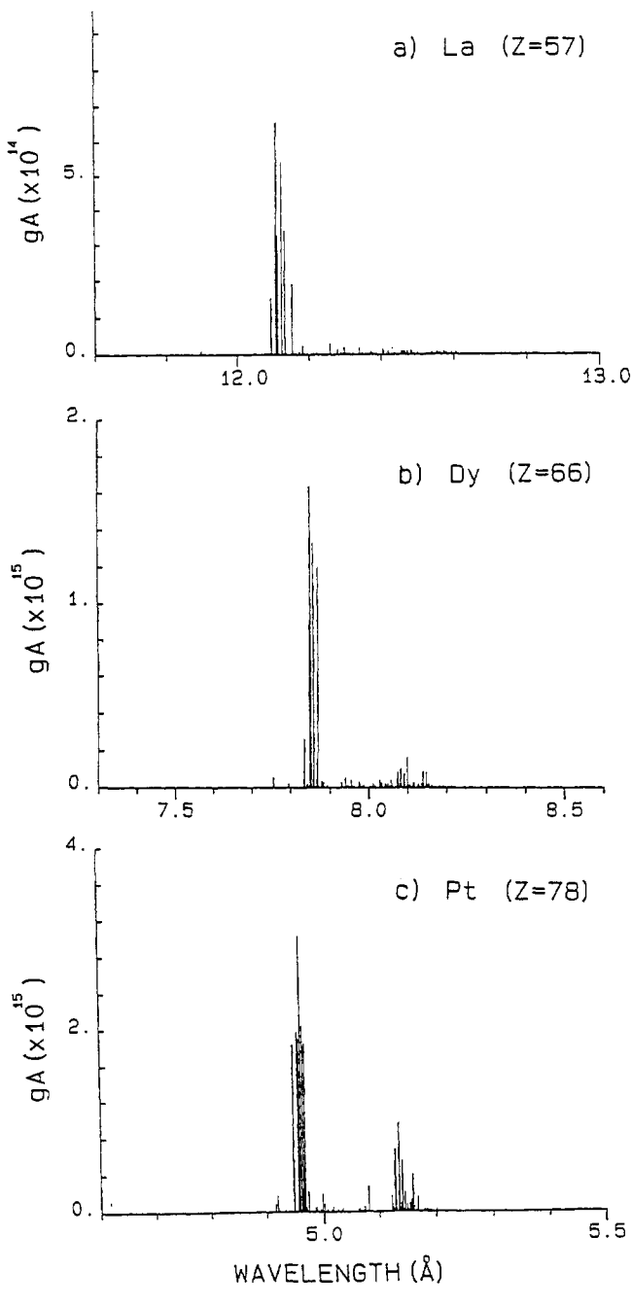

Fig. 3. Synthetic spectra showing the result of the computations of the $3d^{10}4d$–$3d^{9}4d4f$ array in Cu I-like La XXIX (a), Dy XXXVIII (b) and Pt XL (c). The clear transition from *LS* to *jj* coupling is apparent in the experimental spectra when comparing the spectra of rare-earths (this work) with the isoelectronic spectra of fifth row elements (see, for example, Ref. [6]).

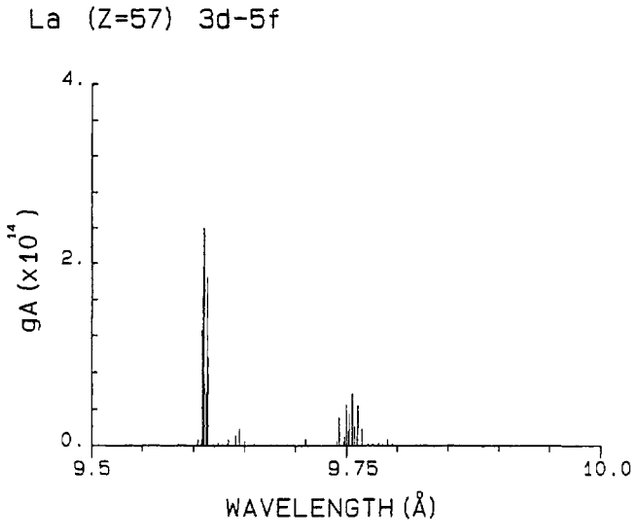

Fig. 4. Synthetic spectra showing the result of the computations of the $3d^{10}4d$–$3d^{9}4d5f$ array in Cu I-like La XXIX. The array is split into two subarrays according to the j value of the $3d$ hole and $5f$ outer electron of the upper excited configuration (see Ref. [19]).

like La ion. All the 14 level energies, electron impact excitation rates at a typical electron temperature of 519 eV (one half the ionization energy of the ion) and the radiative dipole decay rates have been calculated using the HULLAC code. The rate equations have then been solved for electron densities from $10^{18}\,\mathrm{cm}^{-3}$ to $10^{23}\,\mathrm{cm}^{-3}$. These results were shown to be very little dependent on the electron temperature. Figure 5 shows the computed relative population of the $3d^{10}4l$ levels ($l = p, d, f$) to the population of the $3d^{10}4s$ ground level. Figure 5 shows that for a typical electron density of $n_e = 10^{21}\,\mathrm{cm}^{-3}$ (a critical density for the Nd-glass laser used in these experiment), the low lying $3d^{10}4l$ levels are almost statistically populated. Thus all the transitions $3d^{10}4l$–$3d^{9}4l4f$, excited from these levels, are expected to appear in the experimental spectrum. All these transitions give rise to line in the same spectral region and have about the same UTA mean wavelength [21] corresponding to feature 38 in the lanthanum spectrum. Therefore, although configuration mixing can move some lines (especially in the case of transitions with $4s$ or $4p$ spectator electron), the bulk of the intensity of the $3d$–$4f$ transition remains in the original wavelength range. Actually, the same conclusion can be reached for the feature 39 (lanthanum spectrum) or 34 in the praseodymium spectrum. These features have been identified as $3d^{10}4l4l'$–$3d^{9}4l4l'4f$ transitions of the Zn I-like ions, although, in this case, also, configuration mixing through $4s4f$–$4p4d$ or $4p4f$–$4d^2$ interaction can move some lines from the central $3d$–$4f$ Zn I-like feature.

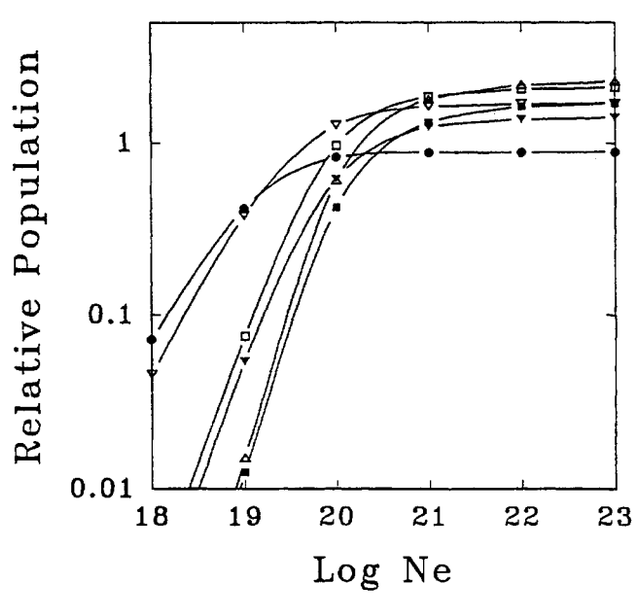

Fig. 5. Population relative to that of the ground state of the La XXIX excited levels $3d^{10}4l_j$ (●, $4p_{1/2}$; ▽, $4p_{3/2}$; ▼, $4d_{3/2}$; □, $4d_{5/2}$; ■, $4f_{5/2}$; △, $4f_{7/2}$). At $n_e = 10^{21}\,\mathrm{cm}^{-3}$, the relative population densities are close to the LTE limit values.

Table III. *Results of* ab-initio *computation of the* $3d^{10}4s$–$3d^{9}4s4f$ *transition in Cu I-like La XXIX (only transitions with* $gf > 0.1$ *are given)*

(a) Results for the $3d^{10}4s$–$3d^{9}4s4f$ transition

Upper level	λ (Å)	gf
0.67 $[3d^9_{3/2}4s(2)4f_{5/2}]1/2$ + 0.32 $[3d^9_{5/2}4s(3)4f_{7/2}]1/2$	12.125	4.10
0.62 $[3d^9_{5/2}4s(3)4f_{7/2}]1/2$ + 0.32 $[3d^9_{3/9}4s(2)4f_{5/2}]1/2$	12.479	0.35
0.40 $[3d^9_{3/2}4s(1)4f_{5/2}]3/2$ + 0.30 $[3d^9_{3/2}4s(2)4f_{5/2}]3/2$	12.118	7.99
0.92 $[3d^9_{3/2}4s(2)4f_{7/2}]3/2$	12.338	0.11
0.25 $[3d^9_{5/2}4s(3)4f_{7/2}]3/2$ + 0.24 $[3d^9_{5/2}4s(2)4f_{7/2}]3/2$	12.467	0.72

(b) Results for the $3d^{10}4s$–$3d^{9}[4s4f + 4p4d]$ transition

Upper level	λ (Å)	gf
0.62 $[3d^9_{3/2}4s(2)4f_{5/2}]1/2$ + 0.33 $[3d^9_{5/2}4s(3)4f_{7/2}]1/2$	12.110	4.02
0.63 $[3d^9_{5/2}4s(3)4f_{7/2}]1/2$	12.499	0.31
0.28 $[3d^9_{3/2}4s(1)4f_{5/2}]3/2$ + 0.17 $[3d^9_{3/2}4s(2)4f_{5/2}]3/2$	12.053	4.79
0.62 $[3d^9_{3/2}4s(2)4f_{7/2}]3/2$	12.279	0.53
0.59 $[3d^9_{5/2}4s(2)4f_{7/2}]3/2$	12.502	0.37
0.23 $[3d^9_{5/2}4s(3)4f_{7/2}]3/2$ + 0.17 $[3d^9_{3/2}4s(2)4f_{7/2}]3/2$	12.420	0.35
0.17 $[3d^9_{3/2}4p_{3/2}(3)4d_{3/2}]3/2$ + 0.13 $[3d^9_{3/2}4s(1)4f_{5/2}]3/2$	12.194	2.73

(a) Single configuration approximation. (b) Including configuration mixing of the upper configuration with $3d^{9}4p4d$.

This simple model shows also that for the Cu I- and Zn I-like $3d$-nf transitions with $n > 4$, each experimental feature is in fact the superposition of many SOSA arising from the different possible spectator electron configurations. But in Tables I and II only the theoretical SOSA with the lowest spectator configuration have been calculated (for example $3d^{10}4s$–$3d^9_{3/2}4s6f_{5/2}$ for the feature labelled 2 in Table I). In fact other SOSA, arising from configurations with other electron configurations (i.e. $3d^{10}nl$–$3d^9_{3/2}nl6f_{5/2}$) might contribute to the line intensity. Since all these SOSAs have approximately the same mean wavelength [21], only the one with the lowest spectator configuration was given in Tables I and II.

5. Conclusion

In this work, a detailed analysis of the X-ray spectrum emitted from the laser produced rare-earths (La and Pr) has been given. Resonance $3d$–nf (n = 4, 5, 6) and $3p$–$4s$, $4d$ transitions of the La XXX and Pr XXXII Ni I-like ions and neighbouring ionization states (La XXVIII to La XXXVI, Pr XXX to Pr XXXVI) have been identified. The effect of configuration mixing was found to be important for the identification of Ni I-like and Cu I-like transitions. The observed satellite spectrum of the Ni I-like $3d^{10}$–$3d^{9}4f$ transition exhibit a pronounced LS structure in contradistinction with the spectra of higher-Z elements which shows a definite jj doubled peak structure.

Table IV. *Results of* ab-initio *computation of the* $3d^{10}4p$–$3d^{9}4p4f$ *transition in Cu I-like La XXIX (only transitions with* $gf > 1.4$ *are given)*

(a) Results for the $3d^{10}4p$–$3d^{9}4p4f$ transition

Upper level	J_G	λ (Å)	gf
0.65 $[3d^9_{3/2}4p_{1/2}(2)4f_{5/2}]1/2$	1/2	12.120	3.88
0.33 $[3d^9_{3/2}4p_{1/2}(1)4f_{5/2}]3/2$	1/2	12.131	7.95
0.60 $[3d^9_{3/2}4p_{3/2}(3)4f_{5/2}]1/2$	3/2	12.100	4.29
0.40 $[3d^9_{3/2}4p_{3/2}(3)4f_{5/2}]3/2$	3/2	12.124	8.06
0.25 $[3d^9_{3/2}4p_{3/2}(2)4f_{5/2}]5/2$	3/2	12.111	11.70

(b) Results for the $3d^{10}4p$–$3d^{9}[4p4f + 4d^2]$ transition

Upper level	J_G	λ (Å)	gf
0.48 $[3d^9_{3/2}4p_{1/2}(2)4f_{5/2}]1/2$ + 0.19 $[3d^9_{5/2}4p_{1/2}(3)4f_{7/2}]1/2$	1/2	12.093	2.75
0.15 $[3d^9_{5/2}4p_{1/2}(2)4f_{7/2}]3/2$ + 0.14 $[3d^9_{3/2}4p_{1/2}(1)4f_{5/2}]3/2$ + 0.11 $[3d^9_{3/2}4p_{1/2}(2)4f_{5/2}]3/2$	1/2	12.106	3.57
0.16 $[3d^9_{3/2}4p_{1/2}(1)4f_{5/2}]3/2$ + 0.13 $[3d^9_{3/2}4p_{1/2}(2)4f_{5/2}]3/2$ + 0.11 $[3d^9_{5/2}\{4d^2_{5/2}(4)\}]3/2$	1/2	12.151	3.03
0.35 $[3d^9_{3/2}4p_{3/2}(3)4f_{5/2}]3/2$ + 0.21 $[3d^9_{3/2}4p_{3/2}(2)4f_{5/2}]3/2$	3/2	12.120	6.82
0.29 $[3d^9_{3/2}4p_{3/2}(1)4f_{7/2}]5/2$ + 0.17$[3d^9_{3/2}\{4d^2_{5/2}(4)\}]3/2$	3/2	12.248	1.48
0.49 $[3d^9_{3/2}4d_{3/2}(0)4d_{5/2}]5/2$ + 0.18 $[3d^9_{5/2}\{4d^2_{5/2}(4)\}]5/2$	3/2	11.964	2.05
0.22 $[3d^9_{3/2}4p_{3/2}(1)4f_{5/2}]5/2$ + 0.17 $[3d^9_{3/2}4p_{3/2}(2)4f_{5/2}]5/2$	3/2	12.120	7.51
0.57 $[3d^9_{3/2}4p_{3/2}(3)4f_{5/2}]1/2$	3/2	12.093	4.19

(a) Single configuration approximation. (b) Including configuration mixing of the upper configuration with $3d^{9}4d^{2}$.

References

1. Zigler, A., Zmora, H., Spector, N., Klapisch, M., Schwob, J. L. and Bar-Shalom, A., J. Opt. Soc. Am. **70**, 129 (1980).
2. Zigler, A., Zmora, H., Spector, N., Klapisch, M., Schwob, J. L. and Bar-Shalom, A., Phys. Lett. **A75**, 343 (1980).
3. Klapisch, M. *et al.*, Phys. Lett. **A79**, 67 (1980).
4. Mandelbaum, P., Klapisch, M., Bar-Shalom, A. and Schwob, J. L., Physica Scripta **27**, 39 (1983).
5. Mandelbaum, P., Klapisch, M., Bar-Shalom, A., Schwob, J. L. and Zigler, A., Phys. Lett. **A99**, 84 (1983).
6. Audebert, P. *et al.*, Phys. Rev. **A32**, 409 (1985).
7. Busquet, M., Pain, D., Bauche, J. and Luc-Koenig, E., Physica Scripta **31**, 137 (1985).
8. Klapisch, M., Mandelbaum, P., Zigler, A., Bauche-Arnoult, C. and Bauche, J., Physica Scripta **34**, 51 (1986).
9. Bauche-Arnoult, C. *et al.*, Phys. Rev. **A33**, 791 (1986).
10. Tragin, N. *et al.*, Physica Scripta **37**, 72 (1988).
11. Burkhalther, P., Nagel, D. and Whitlock, R., Phys. Rev. **A9**, 2331 (1974).
12. Bailey, J., Kilkenny, J. D., Lee, Y., Maxon, S., Schofield, J. H. and Weber, D., Phys. Rev. **35**, 2578 (1987).
13. Von Goeler, S. *et al.*, J. de Phys. C1, **49**, 181 (1988).
14. Renaudin, P. *et al.*, in: "Proceedings of the Xth International Colloquium on UV and X-Ray Spectroscopy of Astrophysical and Laboratory Plasma" (Edited by H. Silver and S. M. Kahn) (Cambridge University Press, Cambridge 1993), p. 156.
15. Mandelbaum, P. *et al.*, Phys. Rev. **A42**, 4412 (1990).
16. Zigler, A., Givon, M., Yarkoni, E., Kishinevsky, M., Golberg, E. and Arad, B., Phys. Rev. **A35**, 280 (1987).
17. Bruneau, J. *et al.*, Phys. Rev. Lett. **65**, 1435 (1990).
18. Klapisch, M., Schwob, J. L., Fraenkel, B. S. and Oreg, J., J. Opt. Soc. Am. **61**, 148 (1977).
19. Bauche-Arnoult, C., Bauche, J. and Klapisch, M., Phys. Rev. **A20**, 2424 (1979).
20. Bauche-Arnoult, C., Bauche, J. and Klapisch, M., Phys. Rev. **A31**, 2248 (1985).
21. Bauche-Arnoult, C. *et al.*, Phys. Rev. **A39**, 1053 (1989).